

TITLE

Virtual environment for manipulating microscopic particles with optical tweezer

Yong-Gu Lee
National Institute of Standards and Technology
100 Bureau Drive, Stop 8262
Gaithersburg, MD 20899-8262
Tel 301-975-3526 Fax 301-975-5118 yglee@nist.gov

Kevin W. Lyons
National Institute of Standards and Technology
100 Bureau Drive, Stop 8263
Gaithersburg, MD 20899-8263
Tel 301-975-6550 Fax 301-258-4482 kevin.lyons@nist.gov

Thomas W. LeBrun
National Institute of Standards and Technology
100 Bureau Drive, Stop 8263
Gaithersburg, MD 20899-8263
Tel 301-975-4256 Fax 301-869-0822 thomas.lebrun@nist.gov

ABSTRACT

In this paper, we use virtual reality techniques to define an intuitive interface to a nanoscale manipulation device. This device utilizes optical methods to focus laser light to trap and re-position nano-to-microscopic particles. The underlying physics are simulated by the use of Lagrange mechanics. We also provide a unique control method for the manipulation of the particles. We let the user naturally grab and steer the particles. Behind the scene, a complex computation is performed to find the new location of the potential field induced by the laser beam that would move the particles accordingly. We use haptic feedback to constrain the steering motion within the physical capability of the potential field.

KEYWORDS

Optical Tweezer, Nanotechnology, Virtual Reality, Nanoscale Assembly

ABBREVIATED ARTICLE TITLE

Virtual Environment for Optical Tweezer

1. INTRODUCTION

The development of nanotechnology [1] has generated a great deal of scientific interest, but the promise of nanotechnology will only be realized by manufacturing commercial products from assemblies of atoms, molecules and nano-scale components. While nanoscale measurement and fabrication techniques are advancing rapidly, few effective techniques for manipulation of nanoscale objects are available. Manipulation of nanoscale objects can be achieved using scanning probe microscopes, such as AFM (Atomic Force Microscope) or STM (Scanning Tunneling Microscope). Guthold et al. [2] performed rolling and sliding of carbon nanotubes using an AFM. Eigler and Schweizer [3] used a STM to position individual xenon atoms on a single-crystal nickel surface, but these tools do not yet offer very articulate control of objects (e.g. the ability to grasp and release). Laser beams can also be used to trap and manipulate small particles. This apparatus is called an OT (optical tweezers) [4], and provides the user with a non-contact method for manipulating objects that can be applied to viruses, bacteria, living cells and synthetic micro and nanoscale particles.

Each method has strengths and weaknesses. The AFM can be used to manipulate a larger set of objects and the relative forces required to manipulate the particles can be more easily derived. The disadvantage is that it is generally less accurate than STM, and since the AFM can directly contact the sample, sharpness and wear of the tool tip considerations must be accounted for. The STM, being non-contact, has little tool wear yet manipulation is limited to conducting and semiconductor materials and typically will occur under vacuum conditions. The strength of OT is that it is well suited for manipulating biological objects, refractive and metallic particles yet it is usually used in solution. The AFM and STM are generally limited to two-dimensions with a very limited third dimension (sometimes referred to as 2.5 dimensions) whilst OT can work in three-dimensions. It is also interesting to note that AFM and STM can work both in imaging and manipulation mode but OT has primarily been used for manipulation, although 3D imaging has been reported [5]. All these techniques require complex driving electronics under sophisticated computer control.

The operation of nanoscale manipulators can be done through tele-operation or automatic manipulation. In the former approach, a human operator acts as a part of the control-loop and issues commands by judgements based on various forms of sensory cues. The sensory cues can be in the form of audio, visual and haptics. In the latter approach, the computer program makes autonomous decisions based on an underlying set of constraints or rules to

perform the predetermined manipulation scenario. In developing these constraints and rules one must have some understanding of nanoscale dynamics yet this is still an emerging field of research. This is why tele-operation is gaining favor for certain user interfaces. Tele-operation needs to virtually present the nanoscale environment to the operator such that the operator can be aware of the target objects and the surroundings. Various techniques in virtual reality can be used to enhance this human-in-the-loop control system by letting the user feel immersed in the environment. Amongst them, haptic display plays a vital role for the following reason.

One of the most difficult problems in nanoscale manipulation is that real-time imaging sensing of nanoscale artifacts is difficult. The imaging sampling time of AFM and STM can take seconds possibly minutes, depending on the scan rate and the sampling range, and can not be done simultaneously with the manipulation. Thus the only real-time feedback occurs with the AFM by way of the force imparted on the probe when sensing (contact or non-contact modes) nanoscale objects or the STM current fluctuations that can be correlated to height of the tip above the surface. The user feedback occurs through linking the AFM force or STM height measurement directly to a haptic device using an appropriate amplification routine. This need for real-time exploration is what attracts researchers to develop man-machine interfaces for nanoscale manipulation that use haptic display technologies. Some of the works are as follows.

Hollis et al. [6] demonstrated that atomic-scale landscapes could be explored and felt with the hand in real time by interfacing a haptic feedback device with an STM. Their haptic device is based on Lorentz magnetic levitation. Sitti and Hashimoto [7] used an AFM with one degree of freedom haptic device to sense nanoscale forces. They demonstrated two-dimensional positioning of micrometer sized latex particles. Guthold et al. [2] used a force feedback device coupled with an AFM tip to haptically sense and manipulate carbon nanotubes, DNA and viruses. All of these research efforts used a graphical display in addition to the haptic display. The topographical data used for the graphical display of the nanoscale objects were acquired by using the probe in the imaging mode that was also used in the manipulation mode. The limitation of this method is that while manipulating the specimen, the graphical display is static and requires additional scans to see the result of the manipulation.

In OT, typical manipulation can be done through two-dimensional pointing devices such as a mouse or joystick. Usually the manipulation is done in non-contact mode, so there is no direct force that can be rendered on a haptic display. Because the ability of traditional optical microscopy to resolve nanometer-scale structures is limited, OT,

unlike AFM or STM, must use other means and synthesize virtual sensory inputs to the operator. This paper presents our work on developing the intuitive interface for manipulating particles through OT with the use of VR (Virtual Reality).

2. APPROACH

We first introduce the Lagrange equation that serves as the foundational model for the trajectory of a particle exposed to a potential field. The potential field is an abstraction of the potential energy field that is induced by the laser beam. Note the potential field depends both on the laser and the particle. For example, if the geometry of the particle changes, the potential field is no longer applicable. Then we derive the equation of potential field position that can be used to steer a particle. Lastly, we present our approach in constraining the steering motion within the physical capability of the optical laser instrument through the use of haptic feedback.

2.1 Modeling of Optical Tweezer Physics

The time required to model the physics associated with the optical tweezer instrument depends on the objective of the work and the accuracies required. Maxwell's equations can be used at the fine level but geometric optics calculations can give sufficient explanations for most cases [8]. Our approach goes one step further and assumes that the potential energy can be represented by an explicit spatial function. For the convenience of implementation we only discuss two-dimensional space and the motions within this space, but this involves no loss of generality for a sphere trapped in a cylindrically symmetric beam.

As an example, let's say we have a spherical particle of radius r , mass m and with a homogeneous material distribution. The form of the trapping potential will depend on the size and properties of both the beam and the particle, as well as the index of refraction of the surrounding medium. To focus on the visualization of trapped particles, we assume a simple potential well with a Gaussian distribution. Assume due to the laser beam, the approximate potential energy of this particle can be given by the following equation.

$$P = -P_0 e^{-\ln(2) \left(\frac{x^2}{a^2} + \frac{y^2}{b^2} \right)} \quad (1)$$

In Eq. (1), P_0 is the well depth, x and y are the two axes perpendicular to the laser path, a and b are the beam waist dimensions. The potential field given in Eq. (1) can be realized by dithering the laser beam or through the use of multiple laser beams. Eq. (1) can be used to describe a spherical potential when a and b are the same or a line potential when one of the beam waist dimension is much greater than the other. Assuming there is no change in the rotational speed of the particle, the kinetic energy of this particle can be given by the following equation.

$$T = \frac{1}{2} m (\dot{x}^2 + \dot{y}^2) \quad (2)$$

From Eq. (1) and (2), Lagrangian Mechanics allows us to predict the behavior of the particle trajectory. The behavior is expressed as a system of n second-order differential equations.

$$\frac{d}{dt} \frac{\partial L}{\partial \dot{q}_i} = \frac{\partial L}{\partial q_i} \quad (3)$$

We define $L = T - P$. In Eq. (3), q_0, q_1, \dots, q_{n-1} and $\dot{q}_0, \dot{q}_1, \dots, \dot{q}_{n-1}$ are the generalized coordinates and the time derivatives of these coordinates. Equivalently,

$$\sum_j \frac{\partial^2 L}{\partial \dot{q}_i \partial \dot{q}_j} \ddot{q}_j + \sum_j \frac{\partial^2 L}{\partial \dot{q}_i \partial q_j} \dot{q}_j = \frac{\partial L}{\partial q_i}.$$

In Cartesian coordinates, above expands to

$$\begin{aligned} \frac{\partial^2 L}{\partial x \partial y} \ddot{y} + \frac{\partial^2 L}{\partial x \partial x} \ddot{x} + \frac{\partial^2 L}{\partial x \partial y} \dot{y} + \frac{\partial^2 L}{\partial x \partial x} \dot{x} &= \frac{\partial L}{\partial x} \\ \frac{\partial^2 L}{\partial y \partial y} \ddot{y} + \frac{\partial^2 L}{\partial y \partial x} \ddot{x} + \frac{\partial^2 L}{\partial y \partial y} \dot{y} + \frac{\partial^2 L}{\partial y \partial x} \dot{x} &= \frac{\partial L}{\partial y} \end{aligned} \quad (4)$$

The Lagrangian of a particle with mass m whose potential is given by Eq. (1) is as follows.

$$L = \frac{1}{2} m (\dot{x}^2 + \dot{y}^2) + P_0 e^{-\ln(2) \left(\frac{x^2}{a^2} + \frac{y^2}{b^2} \right)} \quad (5)$$

Substituting the above Lagrangian to Eq. (4) leads to following differential equations.

$$\begin{aligned}
& \frac{\partial}{\partial \dot{x}} (m \dot{y}) \dot{y} + \frac{\partial}{\partial \dot{x}} (m \dot{x}) \dot{x} + \frac{\partial}{\partial \dot{x}} \left(\frac{-2 \ln(2) P_0 y}{b^2} e^{-\ln(2) \left(\frac{x^2 + y^2}{a^2 + b^2} \right)} \right) \dot{y} + \frac{\partial}{\partial \dot{x}} \left(\frac{-2 \ln(2) P_0 x}{a^2} e^{-\ln(2) \left(\frac{x^2 + y^2}{a^2 + b^2} \right)} \right) \dot{x} \\
&= \frac{-2 \ln(2) P_0 x}{a^2} e^{-\ln(2) \left(\frac{x^2 + y^2}{a^2 + b^2} \right)} \\
& \frac{\partial}{\partial \dot{y}} (m \dot{y}) \dot{y} + \frac{\partial}{\partial \dot{y}} (m \dot{x}) \dot{x} + \frac{\partial}{\partial \dot{y}} \left(\frac{-2 \ln(2) P_0 y}{b^2} e^{-\ln(2) \left(\frac{x^2 + y^2}{a^2 + b^2} \right)} \right) \dot{y} + \frac{\partial}{\partial \dot{y}} \left(\frac{-2 \ln(2) P_0 x}{a^2} e^{-\ln(2) \left(\frac{x^2 + y^2}{a^2 + b^2} \right)} \right) \dot{x} \\
&= \frac{-2 \ln(2) P_0 y}{b^2} e^{-\ln(2) \left(\frac{x^2 + y^2}{a^2 + b^2} \right)}
\end{aligned}$$

Rearranging above leads to following equation.

$$\begin{aligned}
m \ddot{x} &= \frac{-2 \ln(2) P_0 x}{a^2} e^{-\ln(2) \left(\frac{x^2 + y^2}{a^2 + b^2} \right)} \\
m \ddot{y} &= \frac{-2 \ln(2) P_0 y}{b^2} e^{-\ln(2) \left(\frac{x^2 + y^2}{a^2 + b^2} \right)}
\end{aligned} \tag{6}$$

Eq. (6) can not be solved analytically and we use a fourth-order Runge Kutta method for solving the differential equation. With the help of Eq. (6), we can simulate the trajectory of a particle. What is more interesting is that we can solve for the new location of the laser trap (center of the potential field) such that it would influence the particle to move in a certain direction within a specific time lapse. This can be used to steer the particle with greater accuracy.

2.2 Steering the Particle

Most of the current work on OT moves the laser trap position to the desired destination of the particle and let the particle drift to the laser position. For light particles or strong lasers, there would be little difference between the center of potential field and the particle. But for heavy particles with low power lasers, there will be noticeable time delay between the two positions. It is much preferable to use low power lasers for many reasons other than being economical. For example, strong lasers can damage the exposed particle. It is also true that the attraction force is not maximum at the center point. By putting the particle in the maximum force region, the steering response time can be

reduced. When particle needs to be moved quickly, our approach puts the particle in these regions to reduce the response time.

With the use of fourth-order Runge Kutta method, the system of differential equations in Eq. (6) can be converted to difference equations given in Eq. (7). Δx and Δy are the displacements of the particle in x , y directions.

$$\begin{aligned}
 \Delta x = & \frac{1}{6} \Delta t \cdot \dot{x} + \frac{1}{3} \Delta t \left\{ \dot{x} - \frac{\log(2) \Delta t P_0 x}{m a^2} e^{-\ln(2) \left(\frac{x^2}{a^2} + \frac{y^2}{b^2} \right)} \right\} + \\
 & \frac{1}{3} \Delta t \left\{ \dot{x} - \frac{\log(2) \Delta t P_0 \left(x + \frac{1}{2} \Delta t \dot{x} \right)}{m a^2} e^{-\ln(2) \left(\frac{\left(x + \frac{1}{2} \Delta t \dot{x} \right)^2}{a^2} + \frac{y^2}{b^2} \right)} \right\} + \\
 & \frac{1}{6} \Delta t \left\{ \dot{x} - \frac{2 \log(2) \Delta t P_0 \left(x + \frac{1}{2} \Delta t \left(\dot{x} - \frac{\log(2) \Delta t P_0 x}{m a^2} e^{-\ln(2) \left(\frac{x^2}{a^2} + \frac{y^2}{b^2} \right)} \right) \right)}{m a^2} e^{-\ln(2) \left(\frac{\left(x + \frac{1}{2} \Delta t \left(\dot{x} - \frac{\log(2) \Delta t P_0 x}{m a^2} e^{-\ln(2) \left(\frac{x^2}{a^2} + \frac{y^2}{b^2} \right)} \right) \right)^2}{a^2} + \frac{y^2}{b^2} \right)} \right\} \\
 \\
 \Delta y = & \frac{1}{6} \Delta t \cdot \dot{y} + \frac{1}{3} \Delta t \left\{ \dot{y} - \frac{\log(2) \Delta t P_0 y}{m b^2} e^{-\ln(2) \left(\frac{x^2}{a^2} + \frac{y^2}{b^2} \right)} \right\} + \\
 & \frac{1}{3} \Delta t \left\{ \dot{y} - \frac{\log(2) \Delta t P_0 \left(y + \frac{1}{2} \Delta t \dot{y} \right)}{m b^2} e^{-\ln(2) \left(\frac{x^2}{a^2} + \frac{\left(y + \frac{1}{2} \Delta t \dot{y} \right)^2}{b^2} \right)} \right\} + \\
 & \frac{1}{6} \Delta t \left\{ \dot{y} - \frac{2 \log(2) \Delta t P_0 \left(y + \frac{1}{2} \Delta t \left(\dot{y} - \frac{\log(2) \Delta t P_0 y}{m b^2} e^{-\ln(2) \left(\frac{x^2}{a^2} + \frac{y^2}{b^2} \right)} \right) \right)}{m b^2} e^{-\ln(2) \left(\frac{x^2}{a^2} + \frac{\left(y + \frac{1}{2} \Delta t \left(\dot{y} - \frac{\log(2) \Delta t P_0 y}{m b^2} e^{-\ln(2) \left(\frac{x^2}{a^2} + \frac{y^2}{b^2} \right)} \right) \right)^2}{b^2} \right)} \right\}
 \end{aligned} \tag{7}$$

Eq. (7) computes the displacement of a particle due to the potential field in Δt . Inversely, with known Δt and the velocity of the particle, we can compute the location of the particle x, y relative to the center of the potential field. In other words, the center of the potential field relative to the particle location that would move the particle in Δt time with the displacement of $(\Delta x, \Delta y)$ is $-x, -y$. To solve for x, y in Eq. (7) we use Newton's method [9]. The key to the success of Newton's method is how good an initial guess we give. The initial guess we use is obtained in the parameter domain x and y . We first divide the domain into square elements. Now for each element we compute the linear segments of the curve satisfying the first part (Δx) of Eq. (7). The linear segments are determined by the signs of Δx at four corner points. This technique is a specialization of the Marching Cubes algorithm [10] applied to two-dimensions. For each element that we find segments satisfying Δx , we once again obtain the second segment set satisfying Δy . At the end, we compute the possible intersection points between the first and the second sets. These intersection points are refined through Newton's method. If the Newton's method does not converge we subdivide the element into smaller sub elements and start the procedure all over again.

2.3 Working Envelope

We define the Working Envelope (WE) as the envelope of displacement vectors a particle can be moved by a potential field. The WE is dynamic in that it changes due to the velocity of the particle and the time lapse until the next control cycle. WE limits the motion of the particle.

The approach we use to compute the WE is numerical. By using the coordinate values at equally spaced regular grid points as the displacement vectors of a particle with certain elapsed time and initial velocity of the particle, we seek to find if solutions to Eq. (7) exist. The grid points where solutions exist form a lump. By connecting the boundary of this lump with a loop composed of line segments, we define the WE. We used Feldman's algorithm [11] for computing the loop pruning the spurious branches. Furthermore, the entire interior set of grid points to the loop are checked to determine if they have solutions. These points with no solution are re-calculated with smaller square elements for computing the initial guess point to see if that would lead to solutions. In cases where this recursive refinement does not lead to a solution, an average of neighboring solutions is used as the solution.

2.4 User interface

The operator steers the particle with a cursor, a small spherical ball that is position controlled by the stylus of the haptic device. The operator moves the cursor to the particle of interest and presses the button attached to the stylus and then the particle is rigidly glued to the cursor. We are now in the steering mode. The system then shows the W E of the particle in question. The W E depends on the time lapse between the user control cycles and the velocity of the particle. The haptic stylus shows no resistance when the particle is moved inside the W E yet encounters a virtual haptic wall when the particle is moved outside the W E. We used simple linear spring model to render the wall. The ellipse in Figure 1 (a) represents W E of the particle at the center. When the commanded displacement of the particle is within the boundary of the W E, such as the two arrows that are inside the ellipse, the operator experiences no reaction force. And the particle is moved to that position indirectly by the movement of the potential field. In Figure 1 (b) however, we see that the commanded displacement is outside the boundary of the W E. In this case the displacement is intersected with the W E and the particle is moved only up to the intersection point. The excess amount of the displacement command (initial displacement command subtracted by the modified displacement command) is used to determine the relative magnitude of the reaction force. This way the operator would sense a virtual wall at the W E. Notice this way the particle would still move when the issuing command is physically incorrect. This maximizes the capability of the optical tweezer.

3. RESULTS

The results are divided into three subsections. Firstly, we gain understanding of the particle trajectory with various experiments. Secondly, we give the numerical results in computing the laser position and W E. Lastly, we present the virtual environment.

3.1 Characteristics of the particle movement

The trajectories of particles in the potential field can be computed by Eq. (7). To gain insight of how the particles would move in the potential field, we plot the trajectories of particles placed in grid points starting from rest. The result is illustrated in Figure 2 (a). We used following constants: $a = 600$ nanometers, $b = 300$ nanometers,

$p_0 = 1.0 \times 10^{-7}$ nanoJoule, $m = 1.0 \times 10^{-12}$ gram s, $\dot{x} = 0$ nanometers/microseconds,

$\dot{y} = 0$ nanometers/microseconds and $\Delta t = 1.0$ microseconds. Also, the grid spacing in Figure 2 is 160 nanometers.

To examine the nonlinear nature of the trajectory, we try the experiment with multiple time steps. The result of using ten time steps totaling to one microsecond is given in Figure 2 (b). It can be seen that more accurate result can be achieved by using multiple time steps. The accurate result however requires more computation time.

The next question we ask ourselves is how far the particles would travel in the given potential field. Figure 3 (a) is the plot of the displacement distance as the function of the particle location from the center of the potential field.

Figure 3 (b) is the plot of iso-contours of each having the same displacement distance. The legend of the distances is shown at the top right corner. Notice that two spots symmetrical to the horizontal axis have maximum displacement. These spots can be important as they dictate the displacement limit of given laser force field. It is also important to note that the center spot of the laser beam shows low displacement distance. The locus of maximum displacements in radial directions is given in Figure 4 (a). The directions were sampled uniformly in increment of 3.6 degrees.

In realistic situations the particles would have velocities. We study the effect of velocities on the particle trajectory.

In Figure 4 (b), we used $\dot{x} = 100$ nanometers/microseconds, $\dot{y} = 100$ nanometers/microseconds. Notice the locus is changed due to the initial velocity of the particle.

In Fig. 3, the particle was initially at rest, kinetic energy being zero. Since the potential energy is higher on the periphery than the center, the combined total energy is higher on the periphery. This means the plot in Fig. 3 depicts particles in different total energy state. We can obtain different plot when we enforce constant total energy. Fig. 5

(a) is the coordinate system we used for the plot. The ellipse denotes the constant potential energy curve. The small black circle lying on the ellipse is the particle with velocity pointing in certain angle ("velocity angle") to the horizontal axis. The position on the curve is determined by the "position angle." Angles in Fig. 5 (b) and (c) are shown in radians. We plot the particle displacement distance by varying the particle position and its velocity direction on constant potential energy ($5.0e-8$ nanoJoule) curve with constant kinetic energy ($5.0e-9$ nanoJoule). The result is shown in Fig. 5 (b). Figure. 5 (c) is the plot of iso-contours of each having the same displacement distance.

3.2 Computing the laser position

Now we come to the most important part, computing the center of the potential field such that a particle at certain initial velocity would displace to required position in given amount of time. The solution of Eq. (7) can be very involved due to the highly non-linear nature of Δx and Δy , especially when Δt is large. We plot Δx and Δy using $\Delta t = 1.3$, $\dot{x} = 100$ nanometers/microseconds, $\dot{y} = 100$ nanometers/microseconds in Figure 6 (a) and (b), respectively. For visual clarity the axes are moved to the bottom left. The origin is actually at the center. In Figure 7, the two small loops aligned vertically at the center are locus of points satisfying $\Delta y = -800$ nanometers. Similarly, the biggest loop are locus of points satisfying $\Delta x = -160$ nanometers. Two intersection points shown in Figure 7 are the two solution points satisfying both conditions. If we extend this spatially and solve for the solutions, we can compute discrete points where the solutions exist or does not exist. For example, when we use the coordinates of regular grid points as Δx , Δy and represent small dots as points where there are no solutions and larger dots for points where there are, we can get Figure 8 (a). The initial guess points were obtained with grid distance equally spaced as shown in Figure 8 (a). The computation took 17 seconds on a Pentium^{*} PC. Notice that we connected the envelope of solvable grid points with line segments. The connected segments form the WE. If we care to use finer grid distance for the initial guess points, we can get more accurate results. Figure 8 (b) is obtained with four times finer resolution and took 288 seconds. Furthermore Figure 8 (c) is obtained with sixteen times finer resolution and took 4591 seconds. Notice there is very little difference from Figure 8 (b) and Figure 8 (c). Formal formulation for optimal grid spacing for the initial guess point is not easy to do. We therefore examine the results as the function of different resolutions and choose the one where the increase in the resolution does not give significantly better solution.

3.3 The virtual environment

Figure 9 (a) illustrates the initial screen of the VE. The descriptions of the graphical objects are as follows. The solid sphere at the center is the particle. It is being illuminated by a dithered laser beam shooting in the direction of the plane. This is shown as ellipse in Figure 9 (a). The small sphere to the left of the particle is the cursor for the operator. When the haptic stylus is moved, the cursor follows accordingly. The particle can only be moved after it

has been grabbed. To grab the particle, the operator moves the cursor to either touch or be inside the particle and presses the button attached to stylus. To release the particle the operator simply releases the button. The diameter of the particle is one micrometer and the grid spacing distance is 2.9 microns. The physical parameters used for the potential field are $a = 600$ nanometers, $b = 300$ nanometers, $p_0 = 1.0 \times 10^{-7}$ nanoJoule, $m = 1.0 \times 10^{-12}$ grams.

Figure 9 (b) illustrates the instant snapshot when the particle is steered to the right and the displacement amount exceeds the physical capability of the potential field. The virtual environment reacts by reacting with force that is in counter direction to the steering motion. Also the amount of force is proportional to the exceeding distance from the WE. Phantom^{*} was used for the haptic output and steering. This was attached to Windows NT^{*} with Pentium^{*} processor and 256 megabytes RAM. The descriptions of the graphical objects are as follows. The arrow direction and length shows the direction and magnitude of the reaction force applied to the haptic stylus. The slender rod with elliptical cross section denotes the dithered laser beam. Finally the closed loop shows the WE. Because it is too small, it is drawn with the scale factor of 100. The WE and its interior solution points are pre-computed before the execution. The bounding box region with range of -100 nanometer to 100 nanometer on each axis was used to compute the WE. The cached data depends upon elapsed time and the initial velocity of the particle. For simplicity and the limitation of the computer memory we used constant cycle time of 0.2 microseconds. The initial velocity of the particle at each axis were varied from -80 to 80 nanometer/seconds in increments of 5.3333 nanometer/seconds. To introduce viscous effect and also to narrow down the range of velocity of the particle to be considered, the velocity was reduced to one tenth at the end of each cycle. The total processor time to compute this in batch process using an SGI Oxy2^{*} with four processors and 1 gigabytes of main memory took 71487.99 seconds (about 20 hours).

-
- Certain commercial equipment, instruments, or materials are identified in this paper to foster understanding. Such identification does not imply recommendation or endorsement by the National Institute of Standards and Technology, nor does it imply that the materials or equipment identified are necessarily the best available for the purpose.

4. DISCUSSION

The discreteness of the WE introduced some jaggedness to the haptic sensation. Recall that the method of computing the WE uses grid points and the smoothness of the WE is directly proportional to the grid distance. The smaller is the grid distance, the smoother is the WE. However, the use of force feedback for constraining the steering motion of the operator that exceeds the laser capability did prove to be a useful method. The reaction force from the haptic device made it natural for the operator to slow down. In one experiment with the haptic feedback off, the distance between the operator cursor and the particle reached up to 3 microns. In other experiment with the haptic feedback on, the distance between the operator cursor and the particle was kept under 0.3 microns. In order to use this VE in tele-operation, much research needs to be done to understand the interaction between the laser beam and the particle and also the particle and the surrounding fluid. More detailed mathematical model for the potential needs to be derived along with extensive experiments to validate the model. Also the viscous effect of the surrounding fluid needs to be taken care of. When the particle is not a simple sphere as used in this article, the orientation of the particle needs to be considered when computing the WE. This means two more variables to represent the orientation needs to be added to the initial three variables (elapsed time, initial velocity in x and y direction).

When we expand the problem domain to three-dimensions, we presume that most approaches used in the two-dimensions could be used without major changes with several exceptions. The method for computing the initial guess point for Eq. (7) can not be extended to three-dimensions and needs a new numerical method. Also the memory requirement can be substantial in three-dimensions. The cached data for the WE uses twenty-eight megabytes. Added dimension (z axis) would easily use one gigabytes. For non-spherical geometry we would also need to add two more dimensions for the orientation. Obviously, more memory efficient representation of the WE needs to be studied.

5. CONCLUSION

Optical tweezer is a new device that has great potential for manipulating nanoscale objects. The non-intrusive nature of the device enables non-destructive manipulation. To better understand the underlying physical nature of the

device, we have designed and implemented a virtual environment that can simulate the physics of the laser beam and particle interactions. The conversion of the system of differential equations to system of difference equations enabled us to precisely control the transient position of the particle. By putting the particle in the maximum force region, we enable the maximum movement with the given laser condition. We also present a new concept called WE (Working Envelope) and a complex numerical technique to compute it. It is shown that WE can prevent the user from issuing physically impossible movement to the particle.

The simulation environment would have more value when it is used in a tele-operation environment. We would have finer position control without ever losing the grip. This requires more sophisticated potential model and experiments.

6. REFERENCE LIST

- [1] National nanotechnology initiative: The initiative and its implementation plan, National Science and Technology Council, (2000).
- [2] Guthold M, Falvo M R, Matthews S W G, Paulson S, Washburn S, Erie D S R, Brooks F P, Taylor R M, Controlled manipulation of molecular samples with the nanoManipulator, IEEE/ASME Transactions on Mechatronics, 5 (2), 189-198 (2000).
- [3] Eigler D M, Schweizer E K, Positioning single atoms with a scanning tunnelling microscope, Nature, 344, 524-536 (1990).
- [4] Ulanowski Z, Optical Tweezers - principles and applications, Proceedings of the Royal Microscopical Society, 36 (1), 7-14 (2001).
- [5] Tischer C, Altmann S, Fisinger S, Horber J K H, Stelzer E H K, Florin E-L, Three-dimensional thermal noise imaging, Applied Physics Letters, 79 (23), 3878-3880 (2001).
- [6] Hollis R L, Salcudean S, Abraham D W, Toward a tele-nanorobotic manipulation system with atomic scale force feedback and motion resolution, in: Proc. IEEE Symposium on Micro Electro Mechanical Systems, Napa Valley, California, (1990). 115-119.

- [7] Sitti, M etin and Hashimoto, Hideki, Teleoperated nano scale object manipulation, Recent advances on mechatronics, Springer-Verlag (1999). 322-335.
- [8] Ashkin A, Forces of a single-beam gradient laser trap on a dielectric sphere in the ray optics regime, Biophysics Journal, 61, 569-582 (1992).
- [9] Press, William H., Flannery, Brian P., Teukolsky, Saul A., and Vetterling, William T., Numerical recipes in C: The art of scientific computing, Cambridge University Press, (1993).
- [10] Lorensen W E, Cline H E, Marching cubes: a high resolution 3D surface construction algorithm, in: SIGGRAPH Computer Graphics Proceeding, (1987). 163-169.
- [11] Feldman, T in, Generating isovalue contours from a pixmap, Graphics gems III, Academic Press (1992). 29-33.

About the Authors.

Yong-Gu Lee is a Guest Researcher at the Manufacturing Engineering Laboratory, National Institute of Standards and Technology, USA. He received a B.S. (1992), M.S. (1994), and Ph.D. (1997) in Mechanical Design and Production Engineering from Seoul National University, Korea. From 1997 to 2000, he was an Advisory Engineer at Samsung SDS and pioneered UnView (STEP visualizer) and 10DR (Virtual dental implant surgery). Some of his work later resulted in a successful spin-off company. His research interests include computer-aided design and manufacturing. His current research activity focuses on virtual reality and nanomanufacturing.

Kevin W. Lyons is a Program Manager with the Manufacturing Engineering Laboratory at the National Institute of Standards and Technology, Gaithersburg, MD. His primary responsibility is directing the Nanomanufacturing Program. The Nanomanufacturing Program's objective is to support U.S. industry in moving nanomanufacturing technologies into production within this decade by concurrently developing the scientific and engineering foundations necessary to support measurements and standards required to achieve effective and validated nanoscale product and process performance. He also continues to manage research projects in Assembly, Virtual Assembly, and Rapid Prototyping. From 1996 through 1999 he served as Program Manager with the Defense Advanced Research Projects Agency (DARPA), where he was responsible for the conceptualization, development, and execution of advanced research and development programs in design and manufacturing. He supervised programs such as Rapid Design Exploration and Optimization (RaDEO), Agile Manufacturing, and Solid Freeform Fabrication and Design Programs. Prior to his government positions, he worked in industry for 15 years. His work entailed various staff and supervisory positions dealing in quality engineering, factory automation, product design and analysis, and engineering marketing.

Captions to illustrations (grouped on a separate sheet or sheets).

Fig. 1: Displacement of the particle

- (a): Within Working Envelope
- (b): Outside Working Envelope

Fig. 2: Trajectories of particles in optical potential field

- (a): One time step of 1 micro second
- (b): Ten time steps of 0.1 micro seconds

Fig. 3: Plot of displacement distances

- (a): Magnitude
- (b): Iso-contours of equal distances

Fig. 4: Locus of maximum displacements in radial directions

- (a): Particle initially at rest
- (b): Particle initially moving

Fig. 5: Plot of displacement distances for constant energy

- (a): Coordinate system
- (b): Magnitude
- (c): Iso-contours of equal distances

Fig. 6: Solution surface

- (a): Plot of Δx
- (b): Plot of Δy

Fig. 7: Solution points

Fig. 8: Working envelope

- (a) 20x20 grid points used for computing the initial guess point
- (b) 80x80 grid points used for computing the initial guess point
- (c) 320x320 grid points used for computing the initial guess point

Fig. 9:

- (a) Initial screen of the virtual environment
- (b) The reaction force experienced by over running the particle

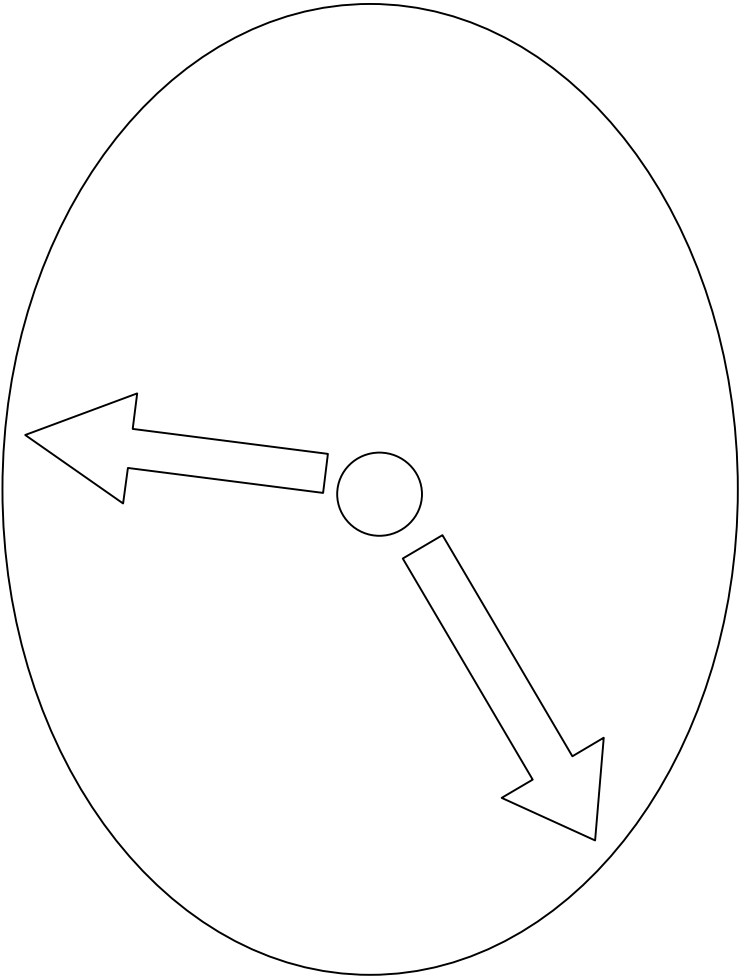


Figure 1 (a) . Journal of Research of the NIST , Yong-G u Lee, K evin Lyons and Thom as Lebrun

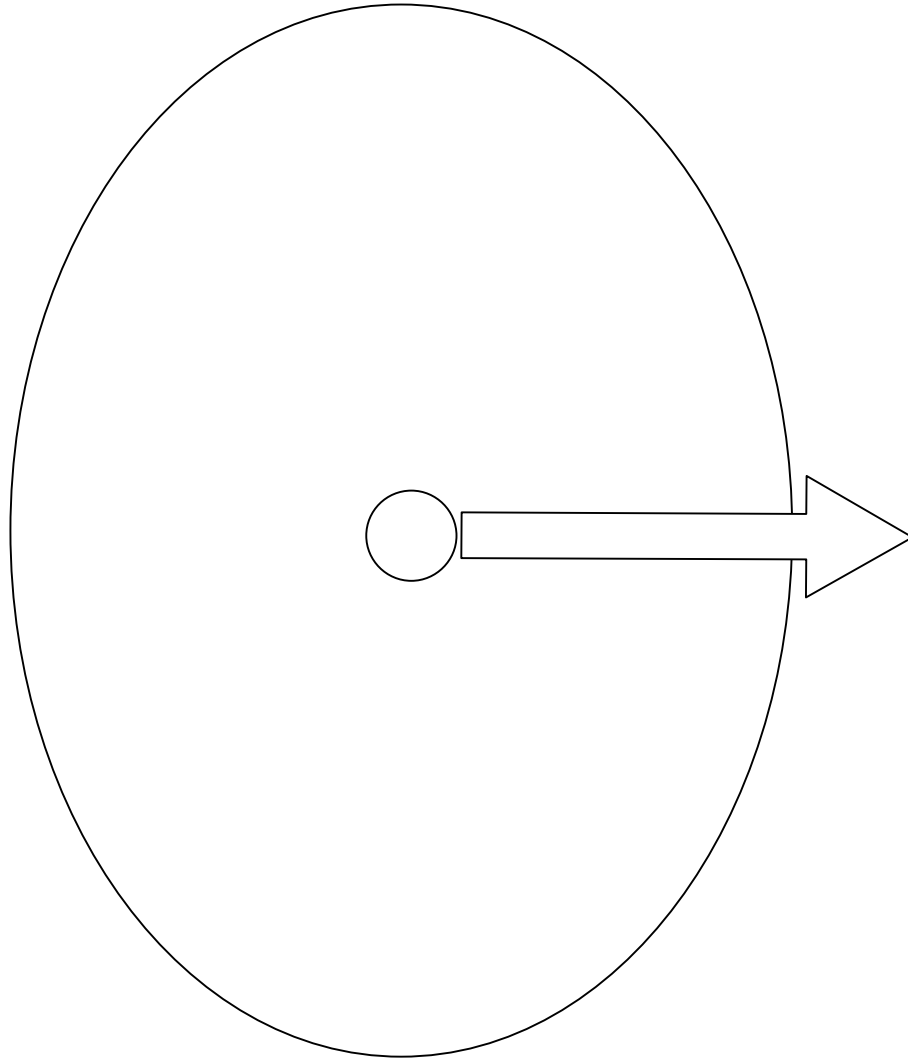


Figure 1 (b). Journal of Research of the NIST, Yong-Gu Lee, Kevin Lyons and Thomas Lebrun

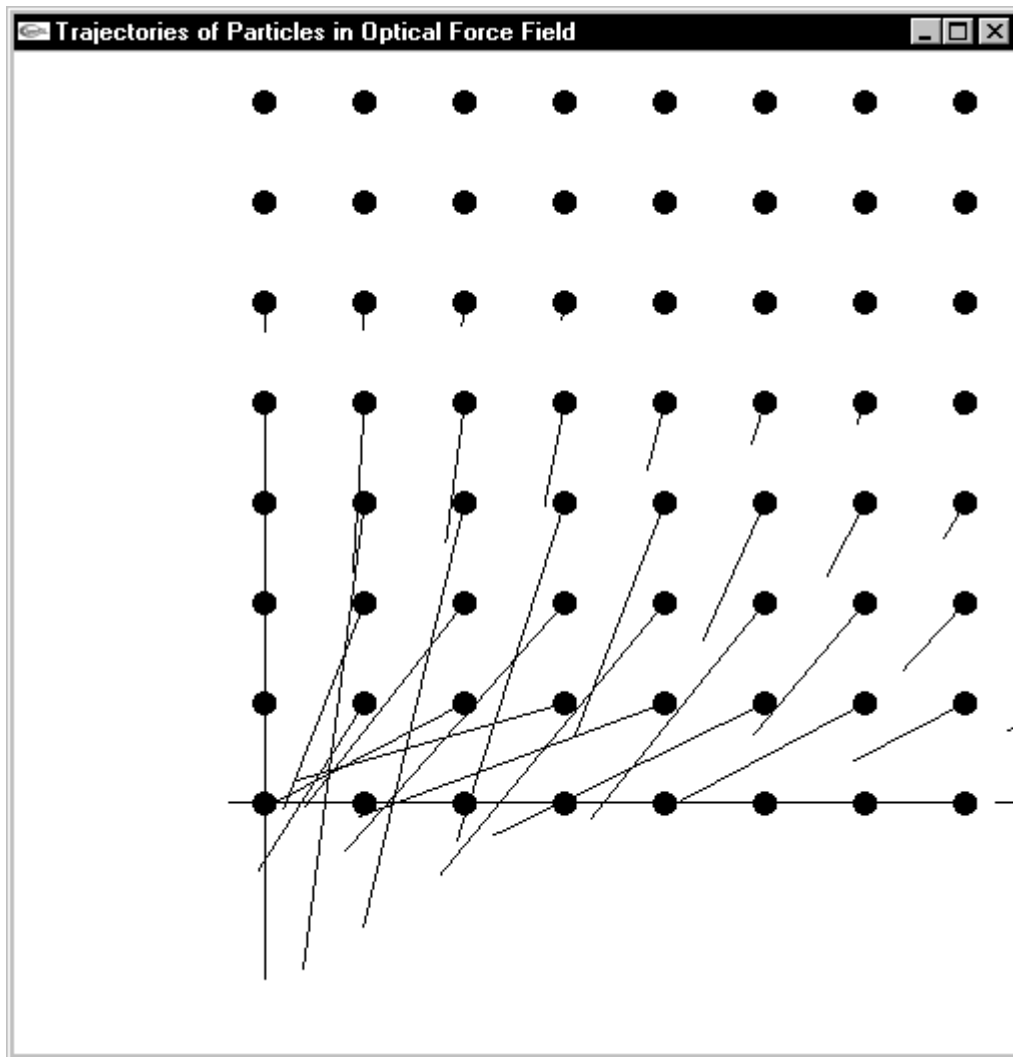


Figure 2 (a) .Journal of Research of the NIST , Yong-Gu Lee, Kevin Lyons and Thomas LeBrun

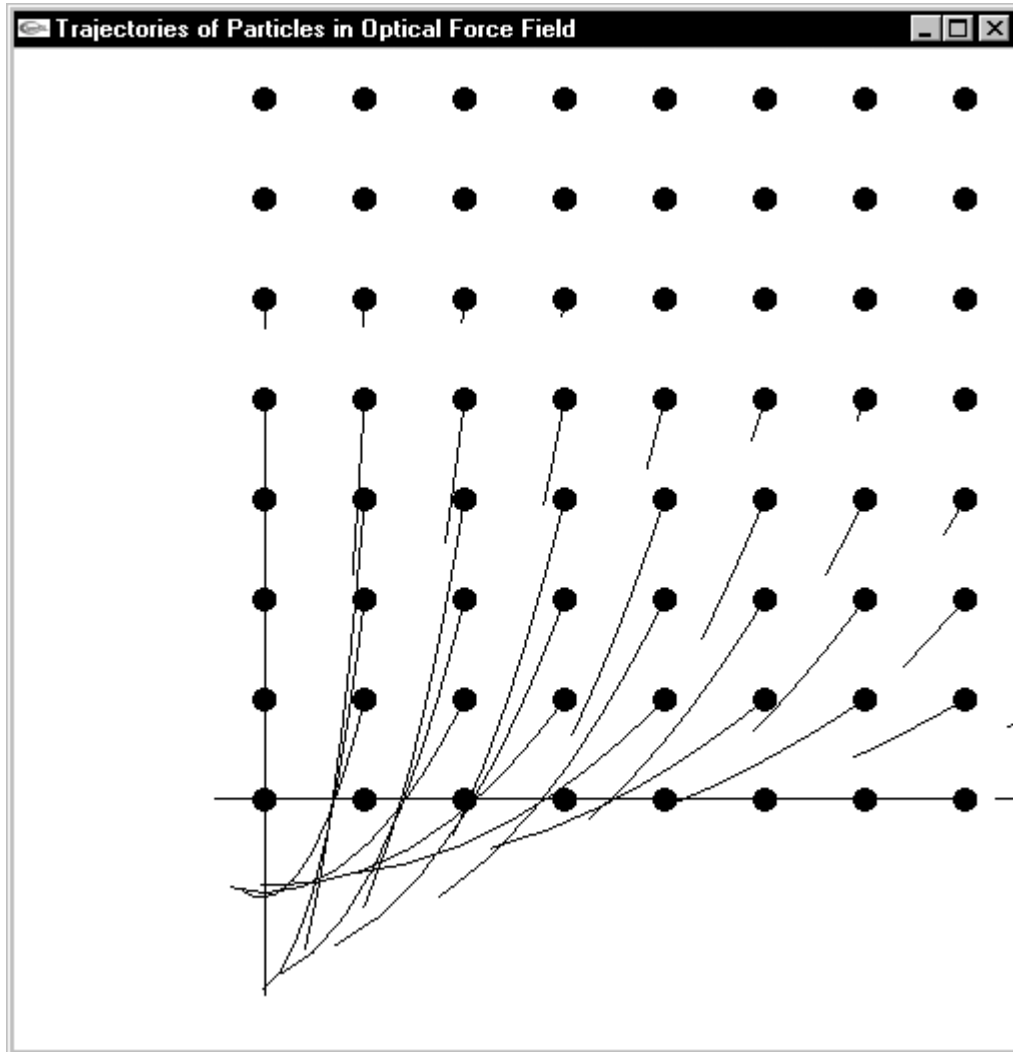


Figure 2 (b). Journal of Research of the NIST, Yong-Gu Lee, Kevin Lyons and Thomas LeBrun

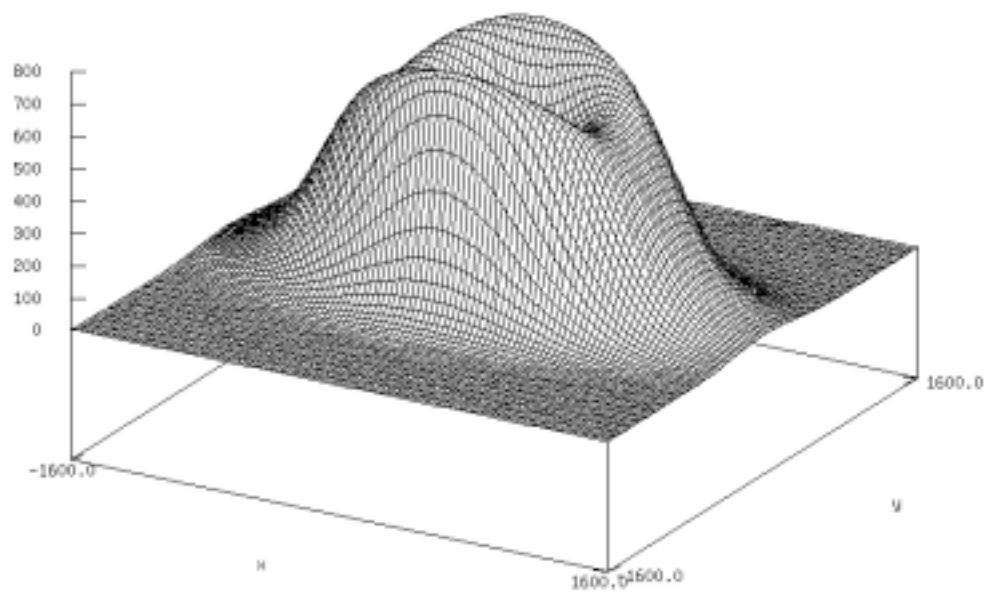


Figure 3 (a). Journal of Research of the NIST, Yong-Gu Lee, Kevin Lyons and Thomas Lebrun

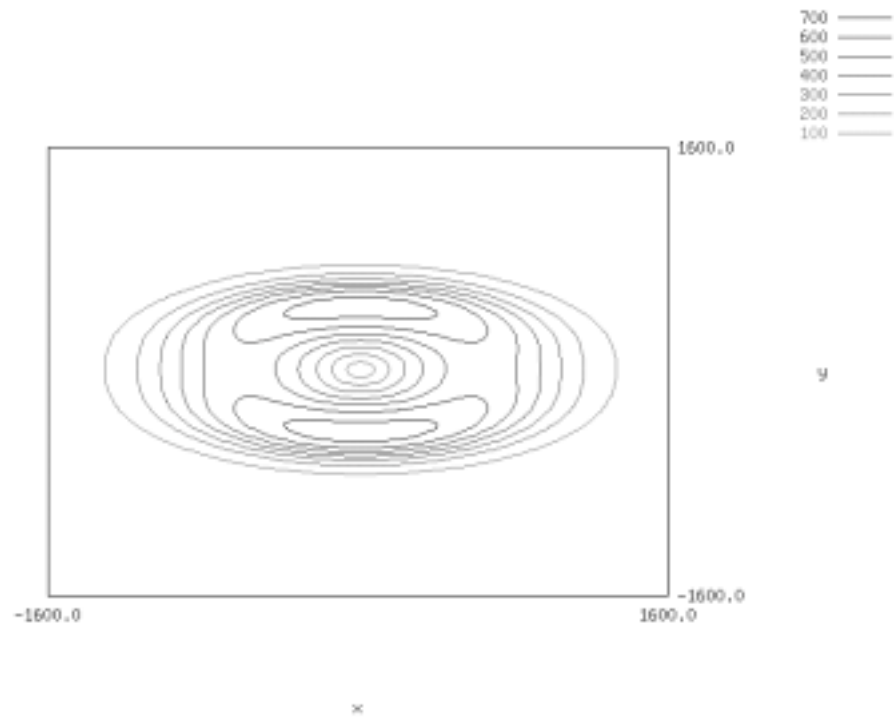


Figure 3 (b). Journal of Research of the NIST, Yong-Gu Lee, Kevin Lyons and Thomas LeBrun

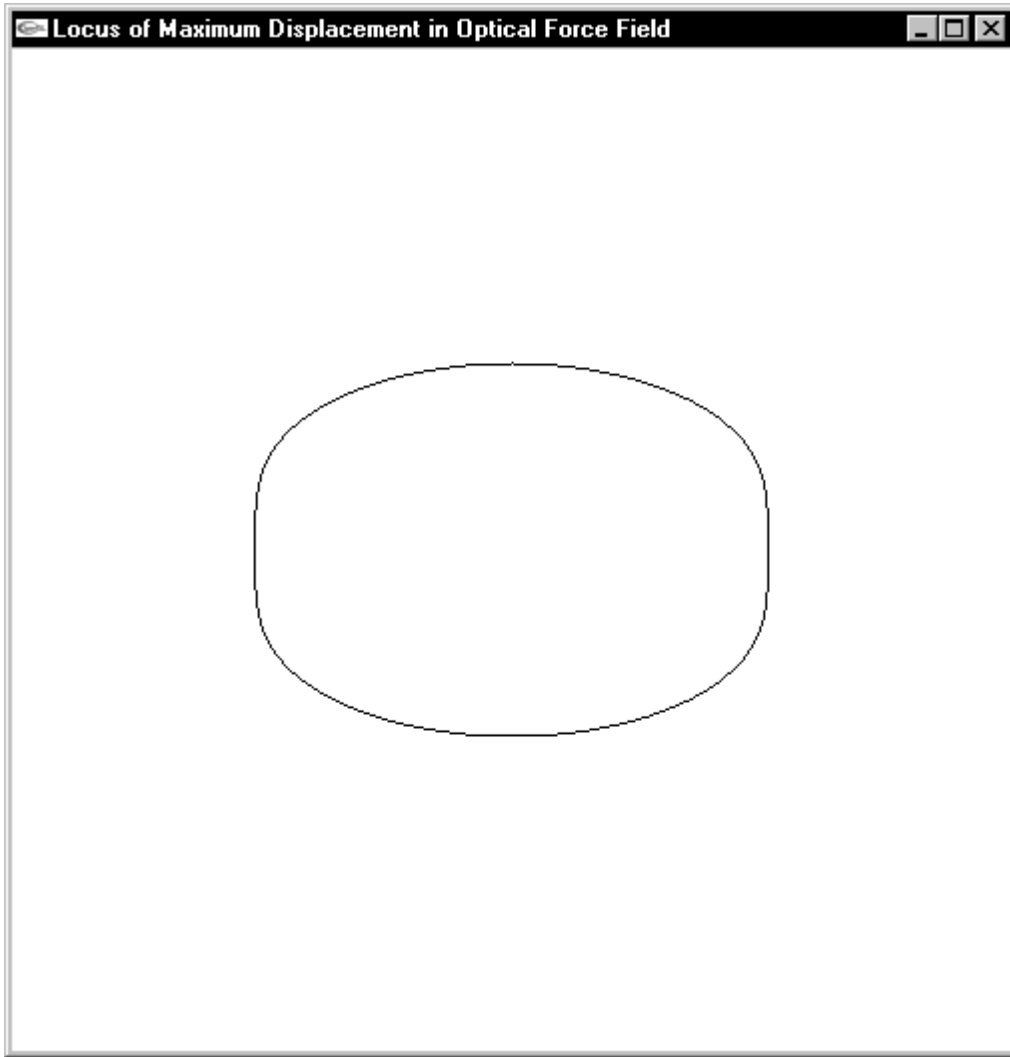


Figure 4 (a). Journal of Research of the NIST, Yong-Gu Lee, Kevin Lyons and Thomas LeBrun

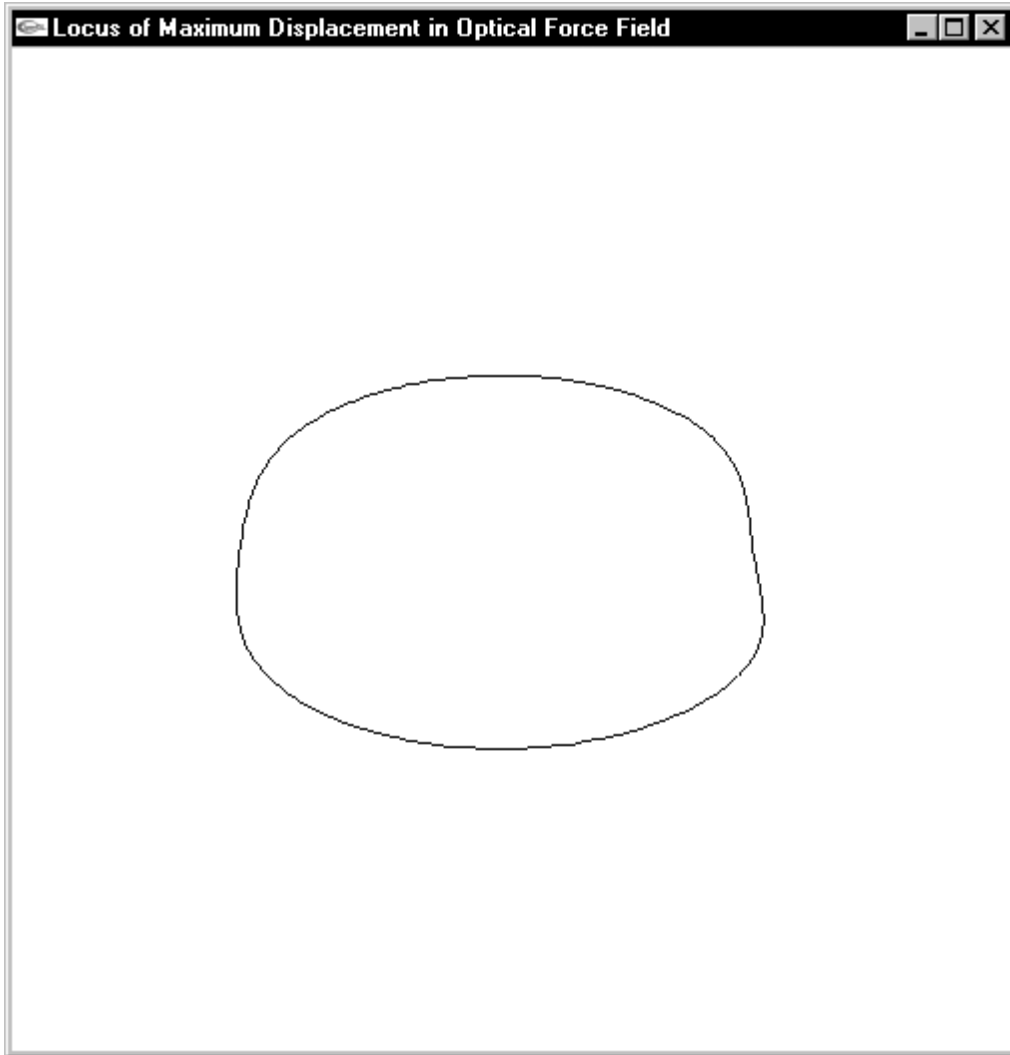


Figure 4 (b). Journal of Research of the NIST, Yong-Gu Lee, Kevin Lyons and Thomas LeBrun

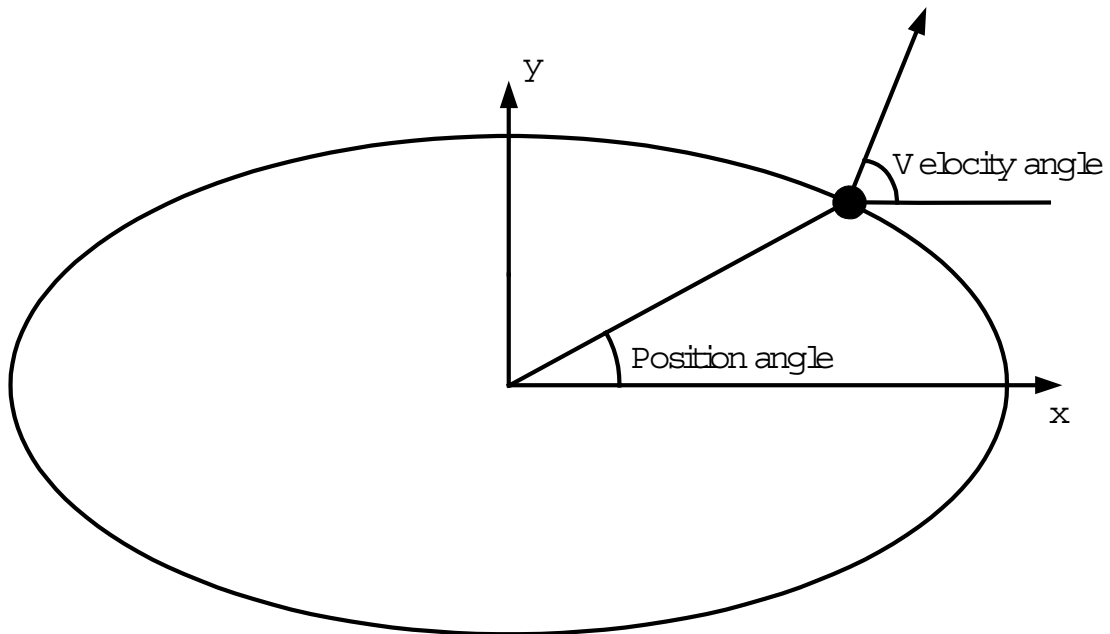


Figure 5 (a). Journal of Research of the NIST, Yong-Gu Lee, Kevin Lyons and Thomas LeBrun

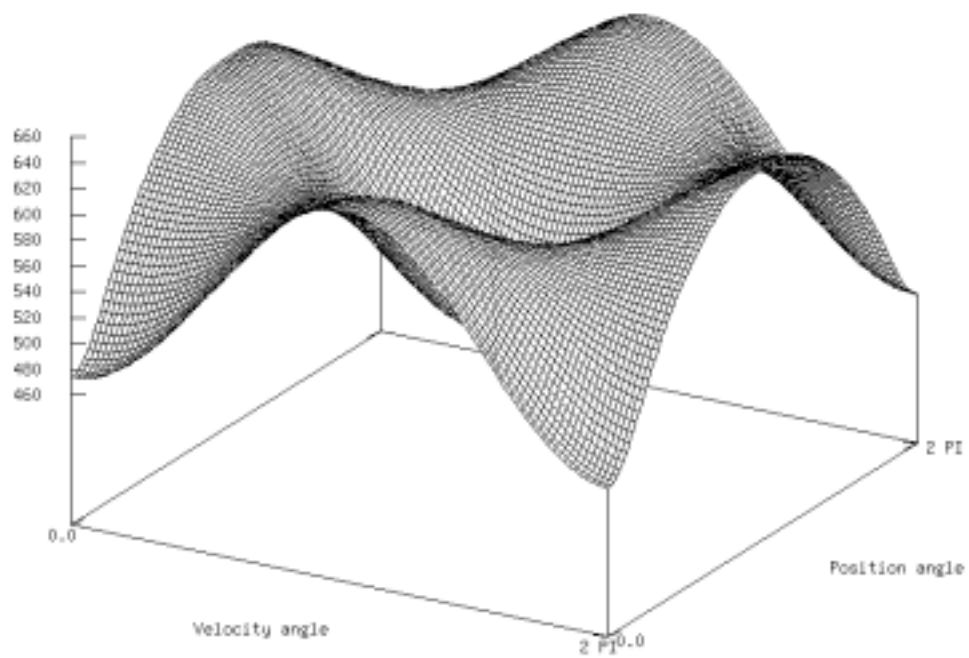


Figure 5 (b). Journal of Research of the NIST, Yong-Gu Lee, Kevin Lyons and Thomas LeBrun

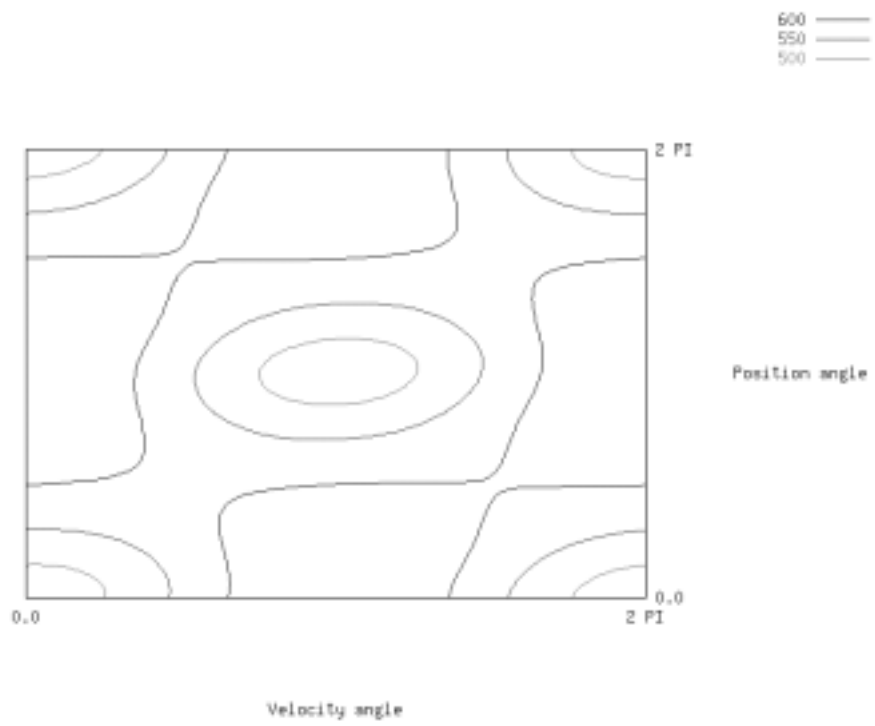


Figure 5 (c). Journal of Research of the NIST, Yong-Gu Lee, Kevin Lyons and Thomas Lebrun

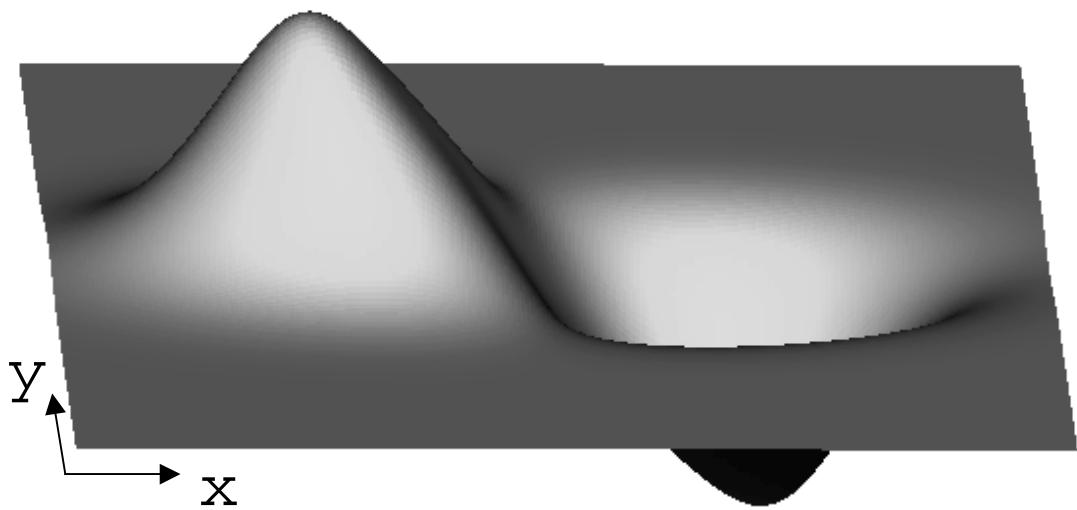


Figure 6 (a). Journal of Research of the NIST, Yong-Gu Lee, Kevin Lyons and Thomas LeBrun

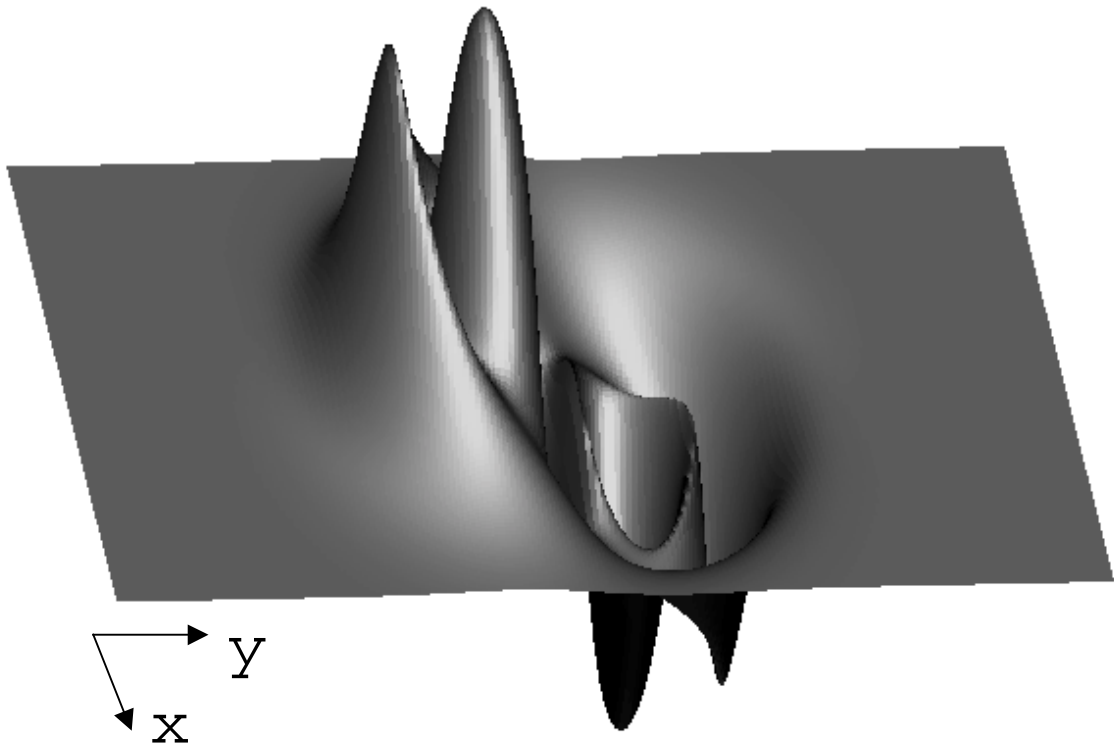


Figure 6 (b). Journal of Research of the NIST, Yong-Gu Lee, Kevin Lyons and Thomas Lebrun

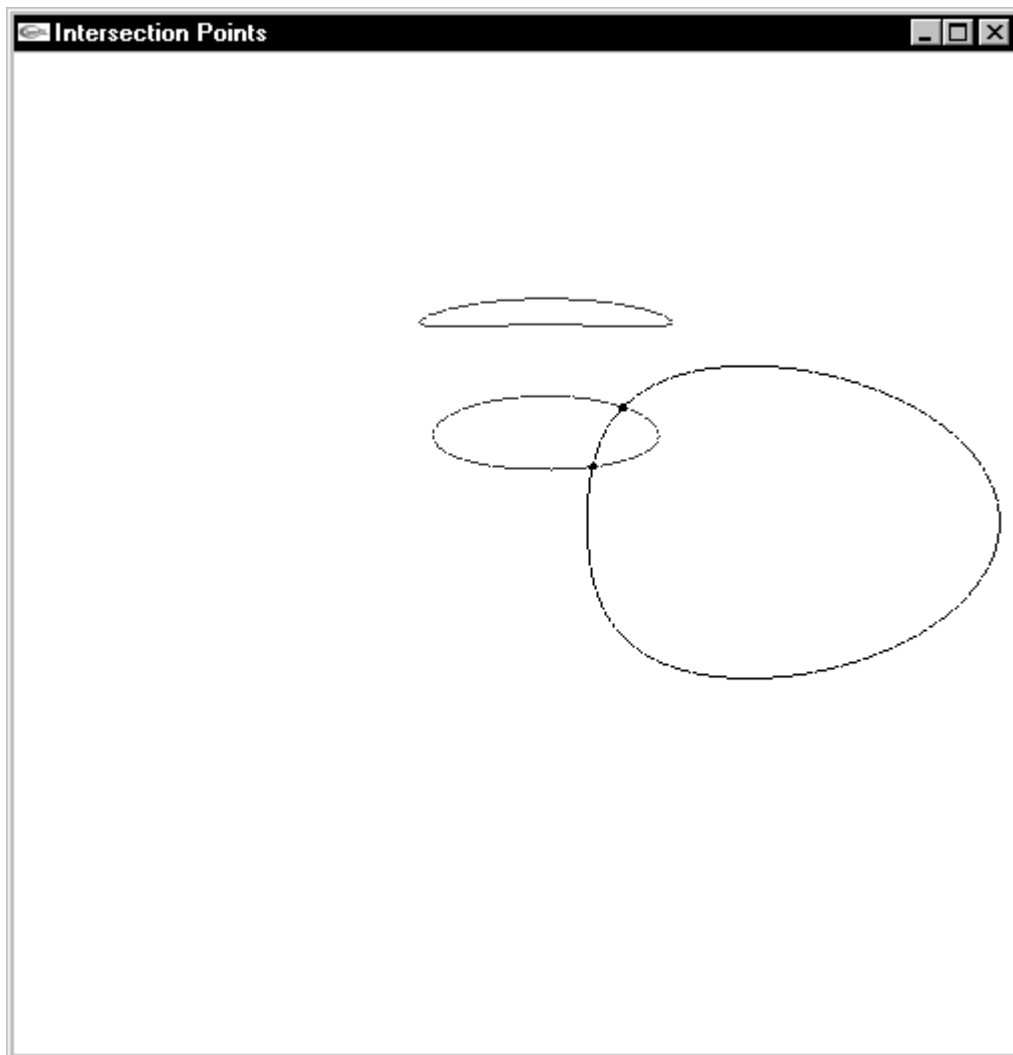


Figure 7. Journal of Research of the NIST, Yong-Gu Lee, Kevin Lyons and Thomas LeBrun

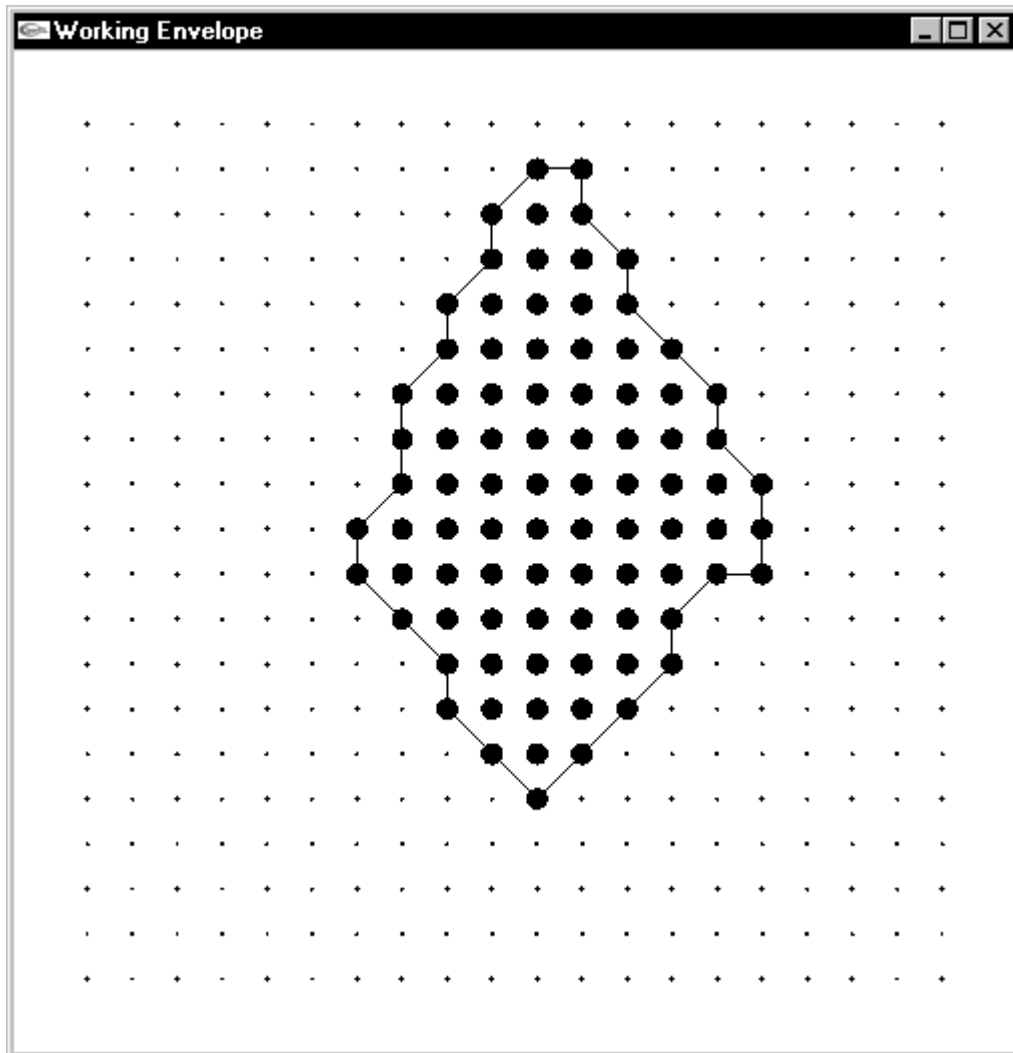


Figure 8 (a). Journal of Research of the NIST, Yong-Gu Lee, Kevin Lyons and Thomas LeBrun

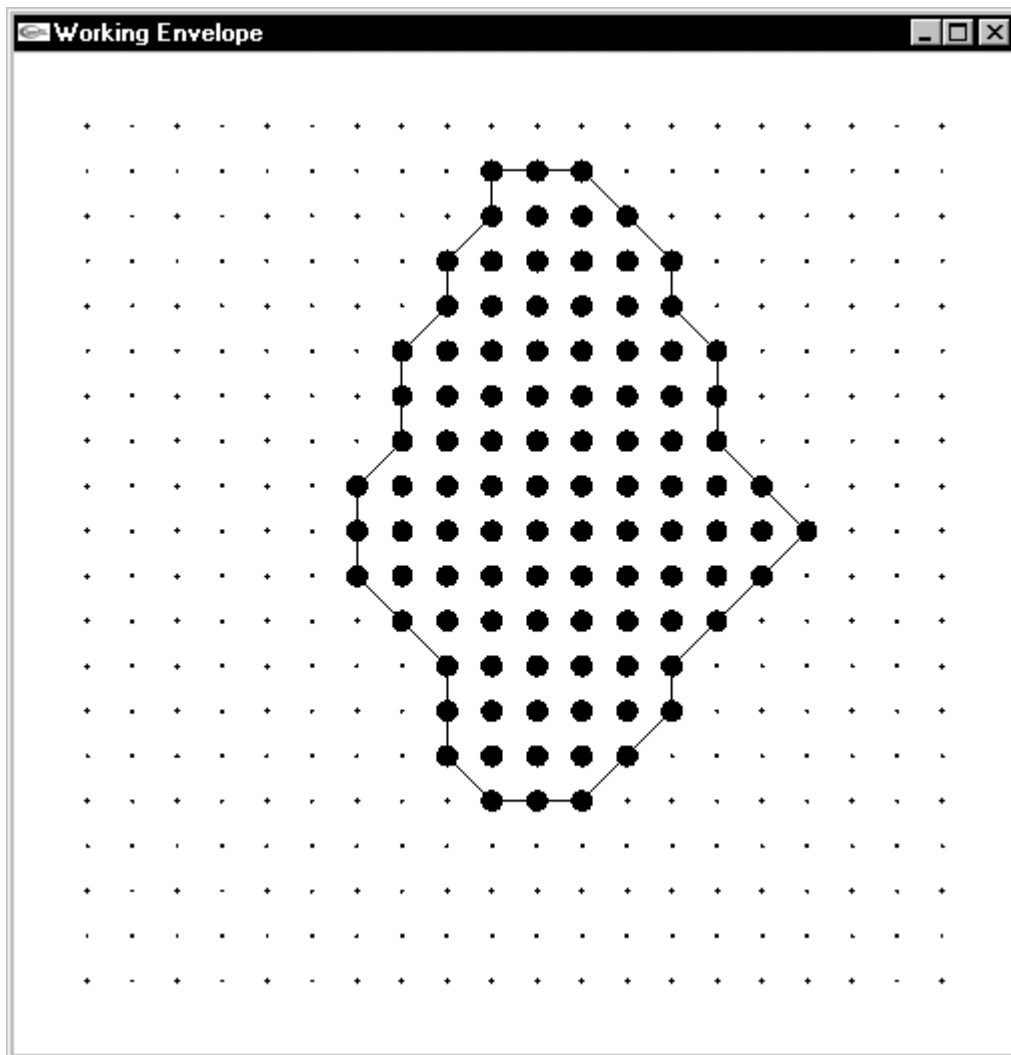


Figure 8 (b). Journal of Research of the NIST, Yong-Gu Lee, Kevin Lyons and Thomas LeBrun

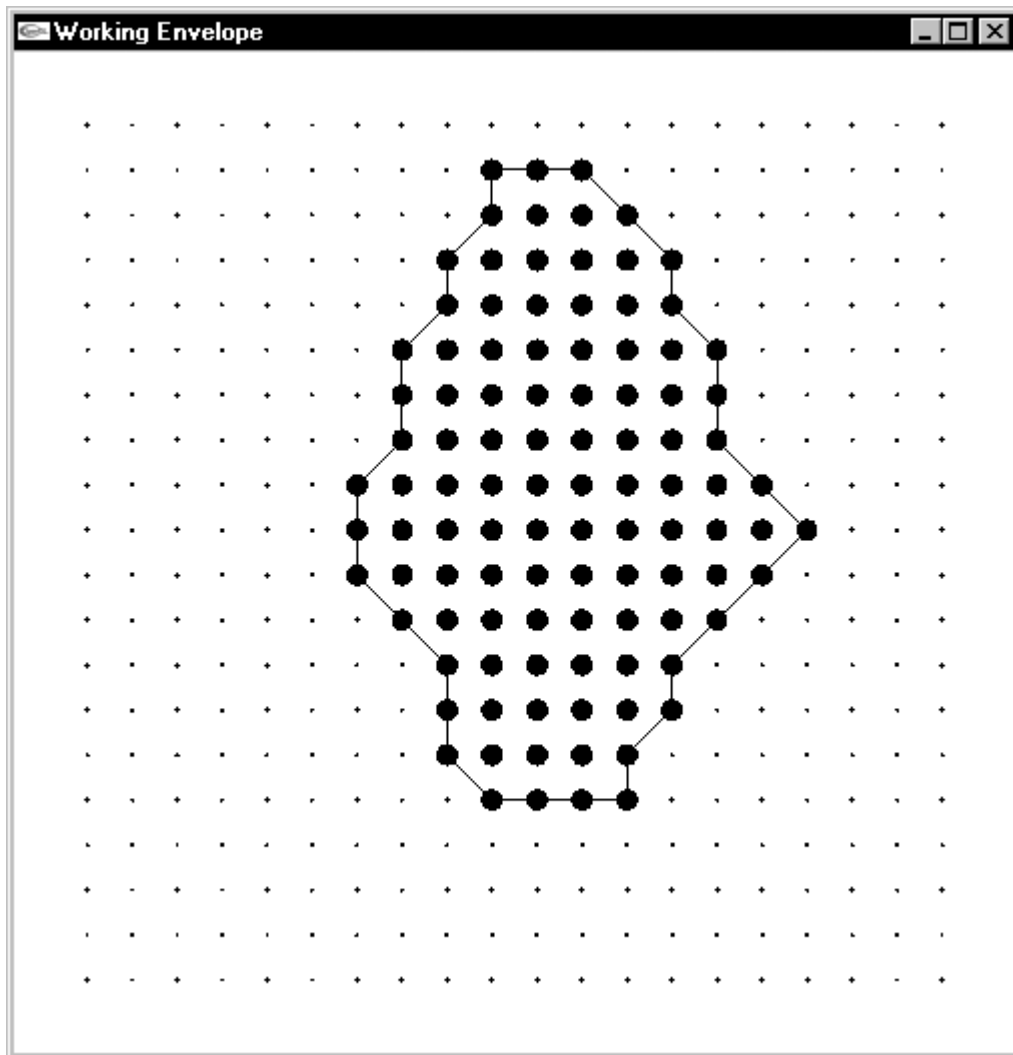


Figure 8 (c). Journal of Research of the NIST, Yong-Gu Lee, Kevin Lyons and Thomas LeBrun

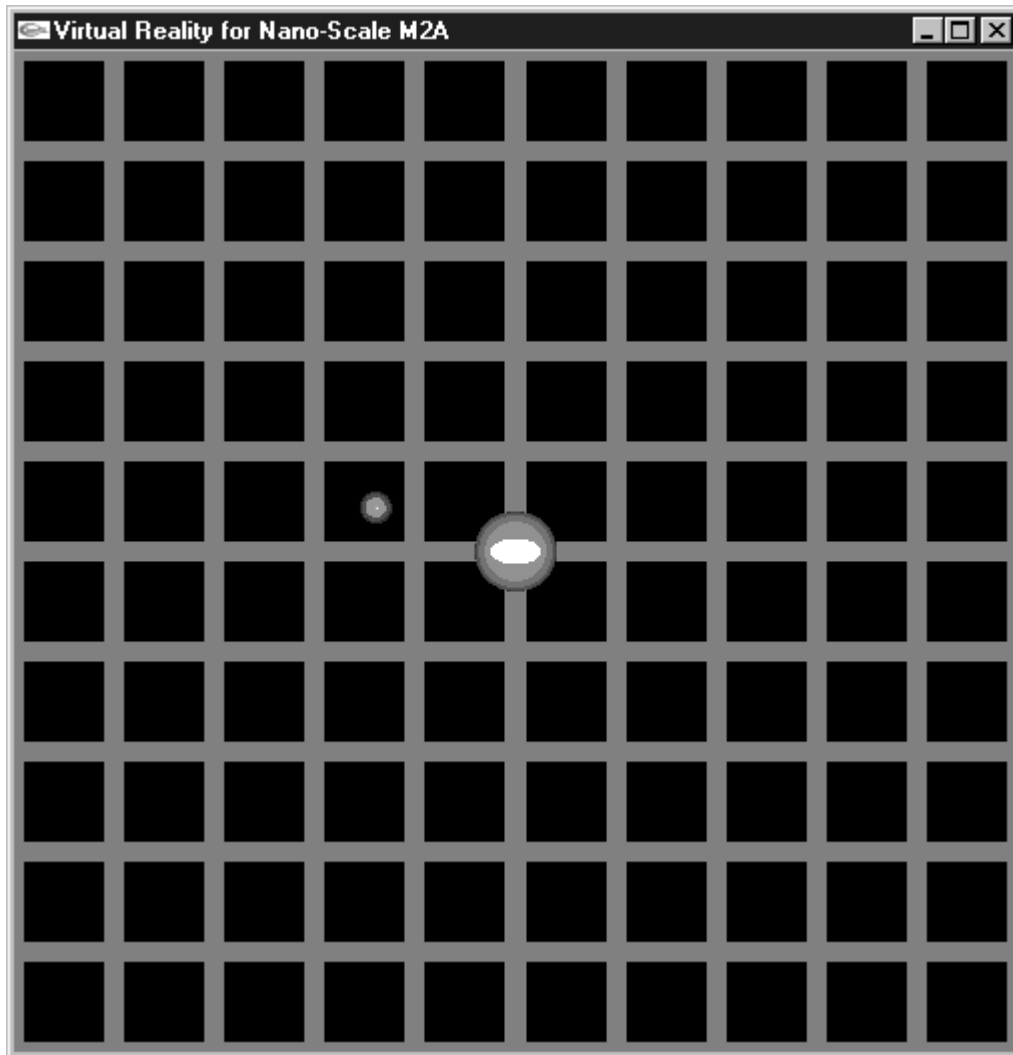


Figure 9 (a). Journal of Research of the NIST, Yong-Gu Lee, Kevin Lyons and Thomas Lebrun

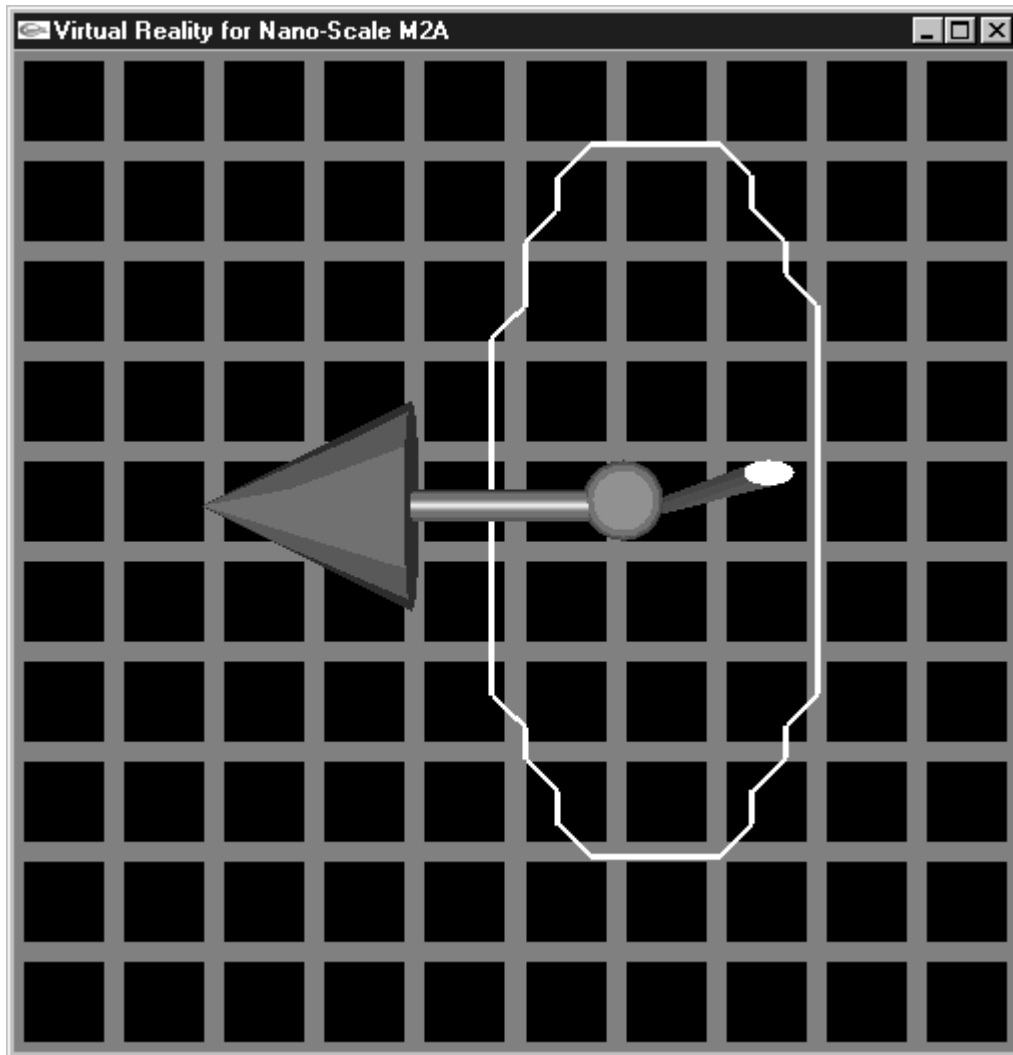


Figure 9 (b). Journal of Research of the NIST, Yong-Gu Lee, Kevin Lyons and Thomas Lebrun